



Jornadas de Jóvenes Investigadores



Aplicación de Nanotubos de Carbono al reforzamiento de materiales compuestos usados en aeronáutica

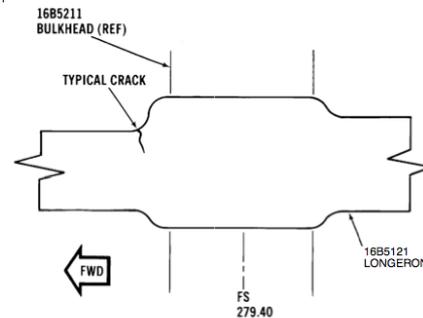
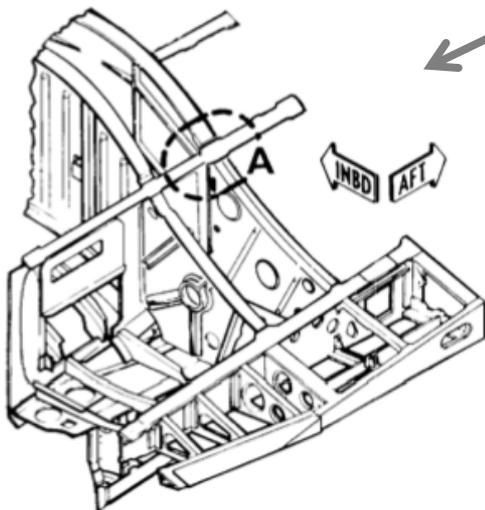
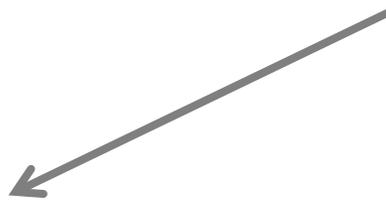
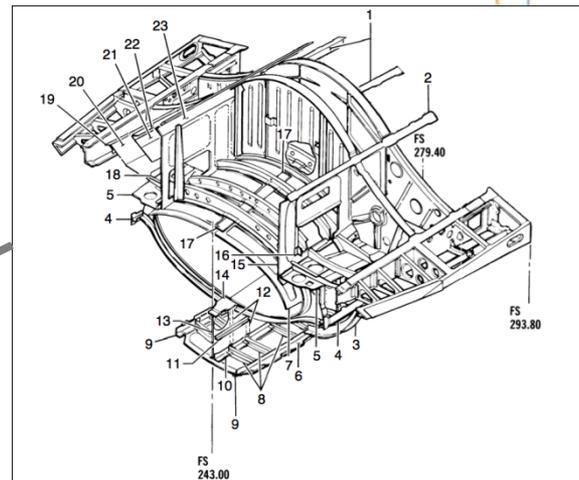
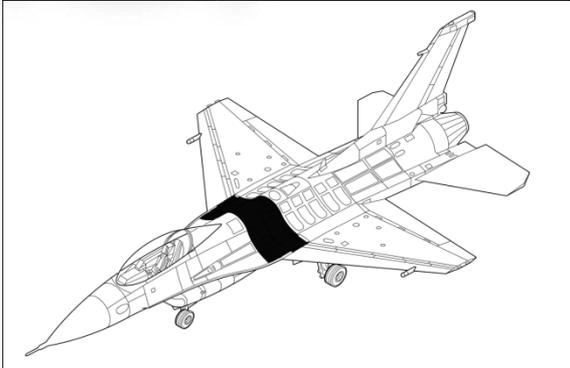
Alberto Monsalve González

alberto.monsalve@usach.cl

Mendoza, 18 de octubre de 2018



INTRODUCCIÓN



VIEW A
(LEFT SIDE SHOWN
RIGHT SIDE OPPOSITE)

Figure 2-110. Repair for 16B5121 Longeron, FS 279.40.

CO-STPM-3-3-213BX99

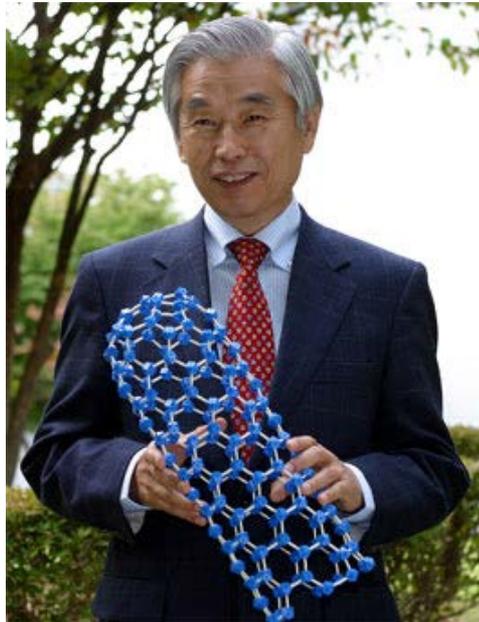




- *Se resumen más de 3 años de investigación en torno al desarrollo de materiales compuestos reforzados con NTC.*
- *Estos materiales son usados como piezas estructurales y como materiales destinados a reparaciones estructurales.*

ANTECEDENTES:

SUMIO IIJIMA, descubridor de los NTC



Helical microtubules of graphitic carbon

Sumio Iijima

NEC Corporation, Fundamental Research Laboratories,
34 Miyukigaoka, Tsukuba, Ibaraki 305, Japan

LETTERS TO NATURE

Helical microtubules of graphitic carbon

Sumio Iijima

NEC Corporation, Fundamental Research Laboratories,
34 Miyukigaoka, Tsukuba 305, Japan

The synthesis of molecular carbon structures in the form of fullerenes and other fullerenes¹ has stimulated interest in the structures accessible to graphitic carbon sheets. Here I report the preparation of a new type of finite carbon structure consisting of needle-like tubes. Produced using an arc-discharge evaporation method similar to that used for fullerene synthesis, the needles grow at the negative end of the electrode used for the arc discharge. Electron microscopy reveals that each needle comprises coaxial tubes of graphitic sheets, ranging in number from 2 to about 50. On each tube the carbon atoms hexagons are arranged in a helical fashion about the needle axis. The helical pitch varies from needle to needle and from tube to tube within a single needle. It appears that this helical structure may aid the growth process. The formation of these needles, ranging from a few to a few tens of nanometres in diameter, suggests that engineering of carbon structures should be possible to create conductors by greater than those relevant to the fullerenes.

Solids of elemental carbon in the sp² bonding state can form a variety of graphitic structures. Graphitic filaments can be produced, for instance, when amorphous carbon filaments formed by thermal decomposition of hydrocarbon species are subsequently graphitized by heat treatment^{2,3}. Graphitic filaments can also grow directly from the vapour-phase deposition of carbon⁴, which also produces soot and other novel structures such as the C₆₀ molecule⁵.

Graphitic carbon needles, ranging from 4 to 16 nm in diameter and up to 4 μm in length, were grown on the negative end of the carbon electrode used in the d.c. arc-discharge evaporation of carbon in an argon-filled vessel (100 Torr). The gas pressure was much lower than that reported for the good carbon-arc discharger⁶ (graphite filaments). The apparatus is very similar to that used for mass production of C₆₀ and C₇₀. The needles seem to grow preferentially on only certain regions of the electrode. The electrode on which carbon was deposited also consisted of intercalated graphite with spherical shell structures, which were 2–20 nm in diameter. The needle structures were examined by transmission electron microscopy (electron energies of 200 kV).

High-resolution electron micrographs of typical needles show 100% lattice images of the graphite structure along the needle axes (Fig. 1). The appearance of the same number of lattice fringes from both sides of a needle suggests that it has a seamless and tubular structure. The thinnest needles, consisting of only two carbon hexagonal sheets (Fig. 1b), are an outer and inner tube, separated by a distance of 0.34 nm, which are 5.5 nm and 4.8 nm in diameter. The separation matches that in bulk graphite. Wall thicknesses of the needles range from 2 to 50 sheets, but thicker tubules tend to be hollowated. The low dimensionality and cylindrical structure are extremely uncommon features in inorganic crystals, although cylindrical crystals such as zeolite⁷ do exist naturally.

The smallest tube observed was 2.2 nm in diameter and was the narrowest tube in one of the needles (Fig. 1c). The diameter corresponds roughly to a ring of 20 carbon hexagons; this small diameter imposes strain on the planar bonds of the hexagons and thus causes two neighbouring hexagons on the ring to meet at an angle of ~6°. For the C₆₀ molecule, the bending angle is 42°, which is much larger than for these tubes. The C–C bond energy calculated for the C₆₀ molecule is smaller than that of graphite⁸, suggesting that bending the hexagons in C₆₀ lowers the bond energy. A similar effect of the bending on bonding energies might apply here. One of the key questions about the tubular structures is how the ABAB hexagonal stacking sequence found in graphite is altered, so it is impossible to figure this clear graphitic structure for coaxial tubes. There would be a shortage of 8 × 9 hexagons in going from one circumference of a tube to that inside it. Disordered graphitic stacking is known as turbostratic stacking, but no detailed accounts of stacking patterns in such structures have been reported. The argument here is also applicable to the spherical graphitic particles, main 'liquid soot'.

All the electron diffraction patterns (Fig. 2) taken from individual carbon needles are indexed by the (h0l) and (hk0) spots for hexagonal symmetry. The patterns always show rings (100) spots when the needle axes are perpendicular to the (001) axis, supporting the idea of a coaxial arrangement of graphitic tubes. As shown in Fig. 2, two side positions of each tube (indicated by shading and labelled 'V') will be oriented so that the



Fig. 1 Electron micrographs of microtubules of graphitic carbon, parallel with the c-axis, showing the (100) lattice images of graphite. A gross effect on the wall thickness is illustrated. a, The cross-section of the graphitic sheet, diameter 0.7 nm. b, The sheet tube, diameter 5.5 nm. c, Seven-sheet tube, diameter 0.5 nm, which has the smallest hollow diameter (2.2 nm).

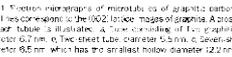


Fig. 2 Electron diffraction patterns of microtubules of graphitic carbon. The patterns always show rings (100) spots when the needle axes are perpendicular to the (001) axis, supporting the idea of a coaxial arrangement of graphitic tubes. As shown in Fig. 2, two side positions of each tube (indicated by shading and labelled 'V') will be oriented so that the

66

© 1991 Nature Publishing Group

NATURE • VOL 354 • 7 NOVEMBER 1991

Nanotubos de Carbono



Refuerzo utilizado
en la resina.



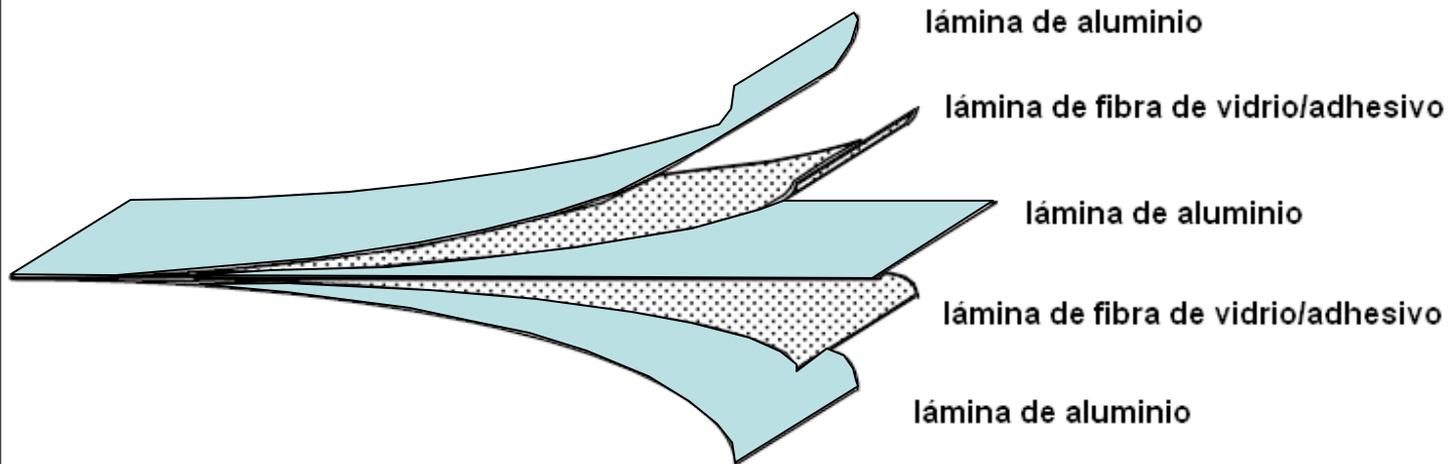
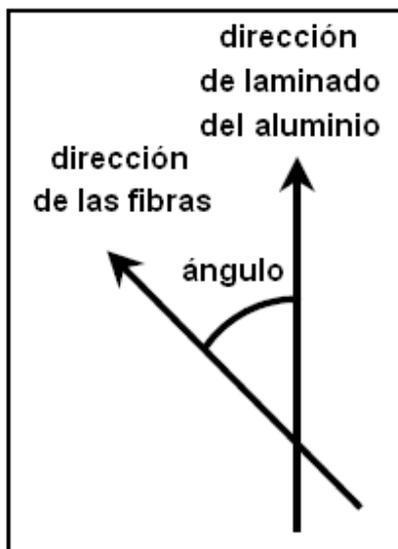
Propiedades	Valor
Diámetro exterior	<20 nm
Diámetro Interior	4 nm
Densidad	2,1 gr/cm ³
Pureza	>99 %
Longitud	1-12 um
Módulo de Elasticidad	950 GPa
Módulo de Corte	400 GPa
Suministro	Polvo seco

NTC a 30000x

MATERIALES INVESTIGADOS:

ARALL (ALUMINIUM ARAMIDE LAMINATE)

GLARE (GLASS ALUMINIUM REINFORCED)



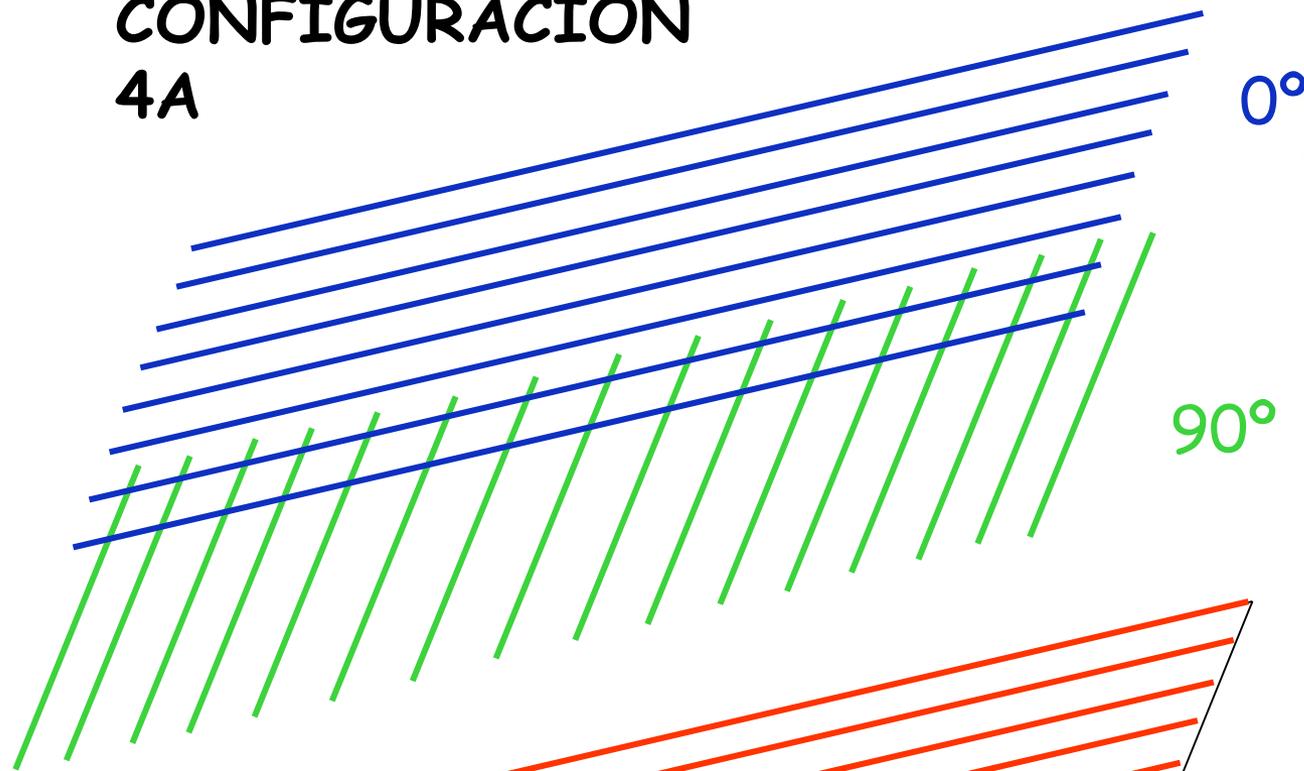
Ejemplo de nomenclatura: GLARE 4A-5/4--4

→ cada lámina de aluminio: $t = 0,4$ mm

→ 5 láminas de aluminio, 4 capas de fibra en configuración GLARE 4

GLARE 4A-5/4-4

CONFIGURACIÓN 4A



CAPAS DE FIBRAS DE VIDRIO

Dirección de laminación de la lámina de Al 2024 T3

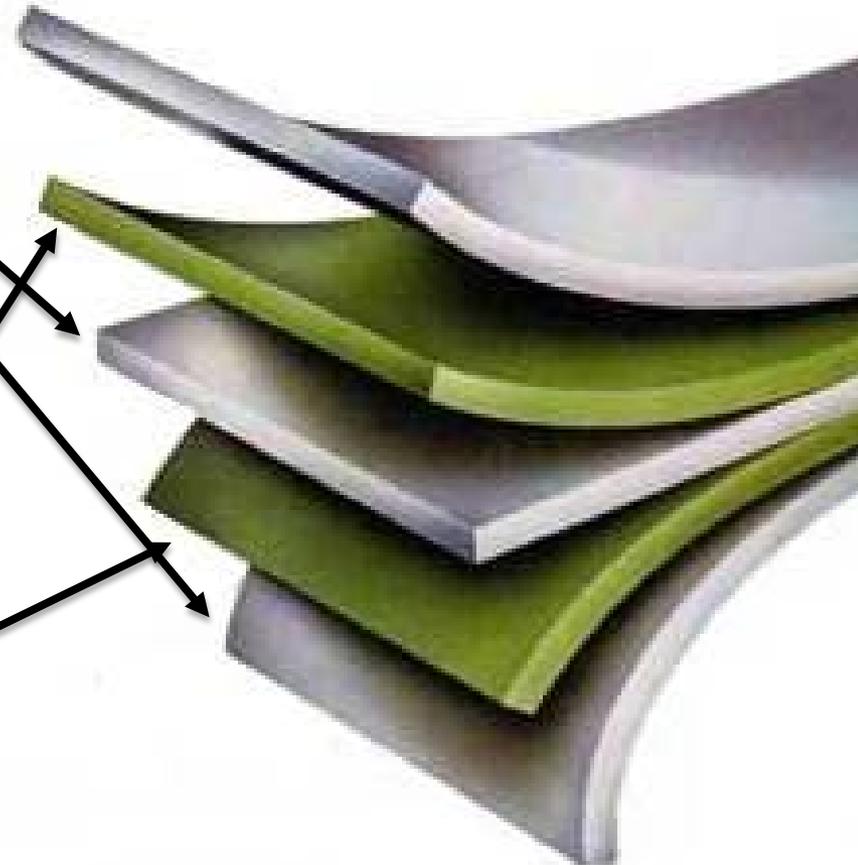
ARALL (ALUMINIUM ARAMIDE LAMINATE)



Aluminio

Resina Epoxi

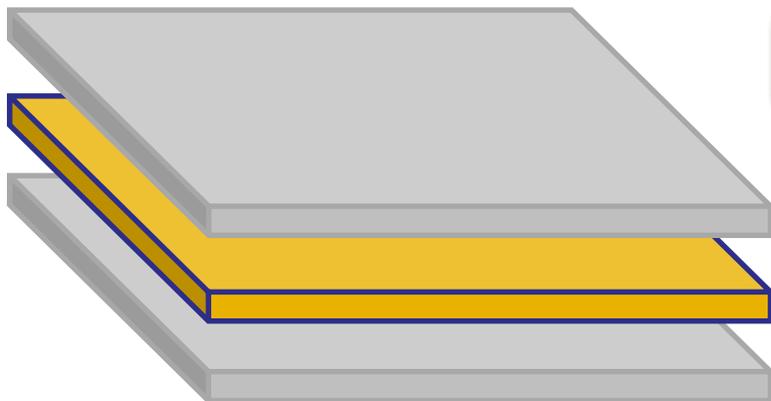
Fibra de
Aramida



DISTINTAS CONFIGURACIONES DE ARALL



Laminado	Espesor del laminado (mm)	Fracción en volumen del metal	Densidad (g/cm ³)
2/1	0,81	0,738	2,35
3/2	1,35	0,679	2,30
4/3	1,88	0,653	2,27
5/4	2,39	0,638	2,24



Laminado 2/1

Espesor del Núcleo: 0,4 mm

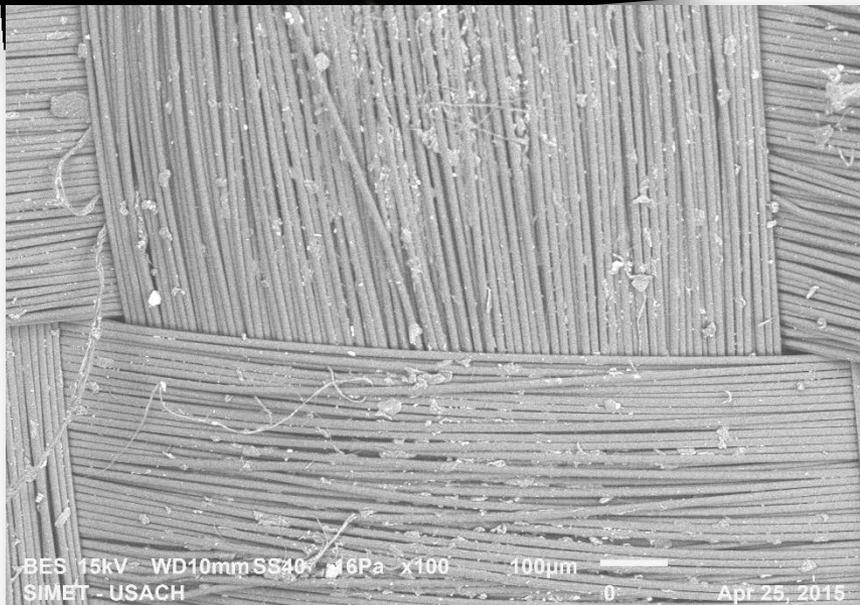
Espesor del Aluminio: 0,55 mm

Fibra de Aramida



**Diámetro
5-15 micrómetros**

Propiedades	Valor
Peso	360 gr/m ²
Espesor	0,4 mm
Max esfuerzo en tensión	2,8 GPa
Absorción de humedad	0,60%
Max Elongación	11%
Módulo de Elasticidad	120 GPa





ANTECEDENTES

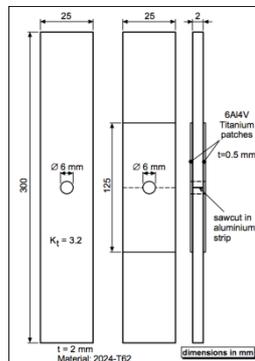
Nationaal Lucht- en Ruimtevaartlaboratorium
National Aerospace Laboratory NLR



NLR-TP-2002-294

Patch repair of cracks in the upper longeron of an F-16 aircraft of the Royal Netherlands Air Force (RNLAf)

W.G.J. 't Hart and J.A.M. Boogers



Australian Government
Department of Defence
Defence Science and
Technology Organisation

Environmental Durability Trial of Bonded Composite Repairs to Metallic Aircraft Structure

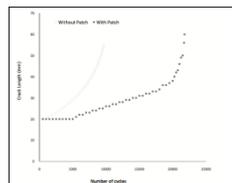
Andrew Rider, Ian Williams Ed Shum and Leo Mirabella

Air Vehicles Division
Platforms Sciences Laboratory

DSTO-TR-1685

Bonded Composite Patch Repairs on Cracked Aluminum Plates: Theory, Modeling and Experiments

Fabrizio Ricci, Francesco Franco and Nicola Montefusco
University of Naples "Federico II", Department of Aerospace Engineering
Italy



REPAIRING GLARE SHEETS SUBJECTED TO BALLISTIC IMPACT

A. Monsalve^(1,2), J. Loyola⁽²⁾, A. Artigas⁽¹⁾, L. Carvajal⁽¹⁾ and O. Bustos⁽¹⁾

(1) Departamento de Ingeniería Metalúrgica, Facultad de Ingeniería, Universidad de Santiago de Chile, Casilla 10233, Santiago, Chile.

(2) Academia Politécnica Aeronáutica, Fuerza Aérea de Chile





Composites Science and Technology 71 (2011) 31–38

Composites Science and Technology 70 (2010) 901–908

ELSEVIER



Contents lists available at ScienceDirect

Composites Science and Technology

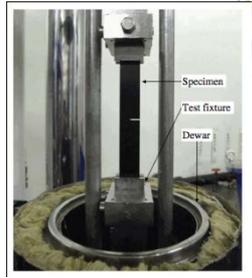
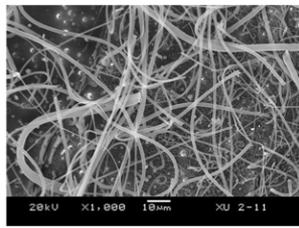
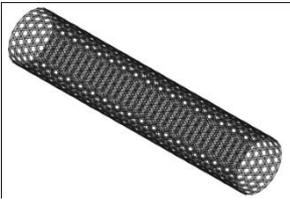
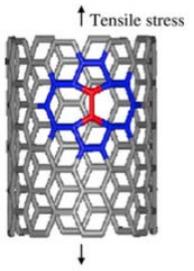
journal homepage: www.elsevier.com/locate/compscitech



Enhancement of delamination fatigue resistance in carbon nanotube reinforced glass fiber/polymer composites

Christopher S. Grimmer, C.K.H. Dharan *

Department of Mechanical Engineering, University of California, Berkeley, CA 94720-1740, USA



ARALL:

SE FABRICÓ EN EL TALLER DE MATERIALES
COMPUESTOS DE LA EMPRESA NACIONAL DE
AERONÁUTICA



FABRICACION DE ARALL Y GLARE



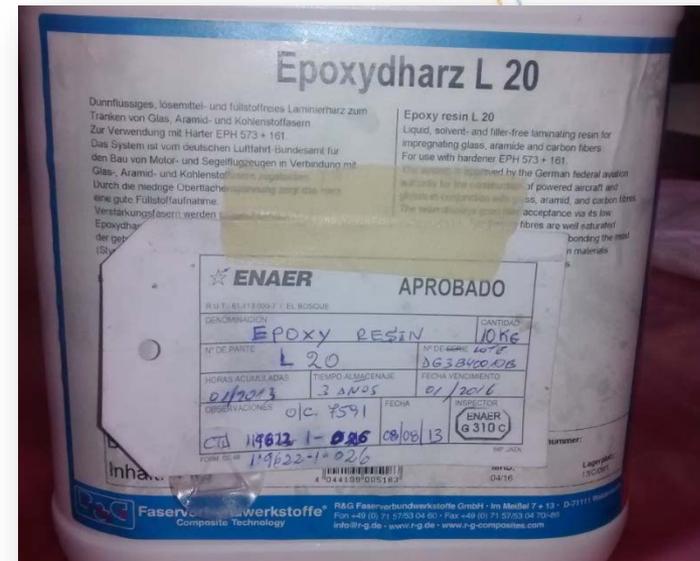
Resina Epoxi

Resina Epoxi L20



Endurecedor EPH 161

Propiedades	Valor
Densidad	1,158 gr/cm ³
Resistencia a Tensión	70,2 MPa
Elongación Máxima	9,5 %
Módulo de Elasticidad	3,4 GPa
Módulo de Corte	1019 MPa



FABRICACIÓN



Configuración 1



50 rpm – 120
seg

FABRICACIÓN

Configuración 2 y 3

Endurecedor



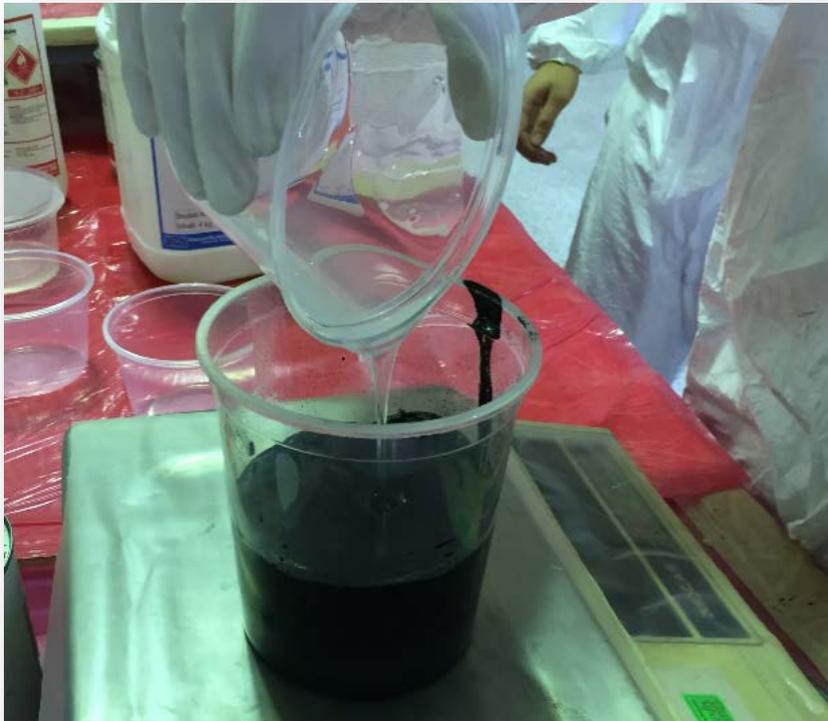
Polvo de NTC

10-15 minutos
Maquina
Ultrasonido
ELMA S30



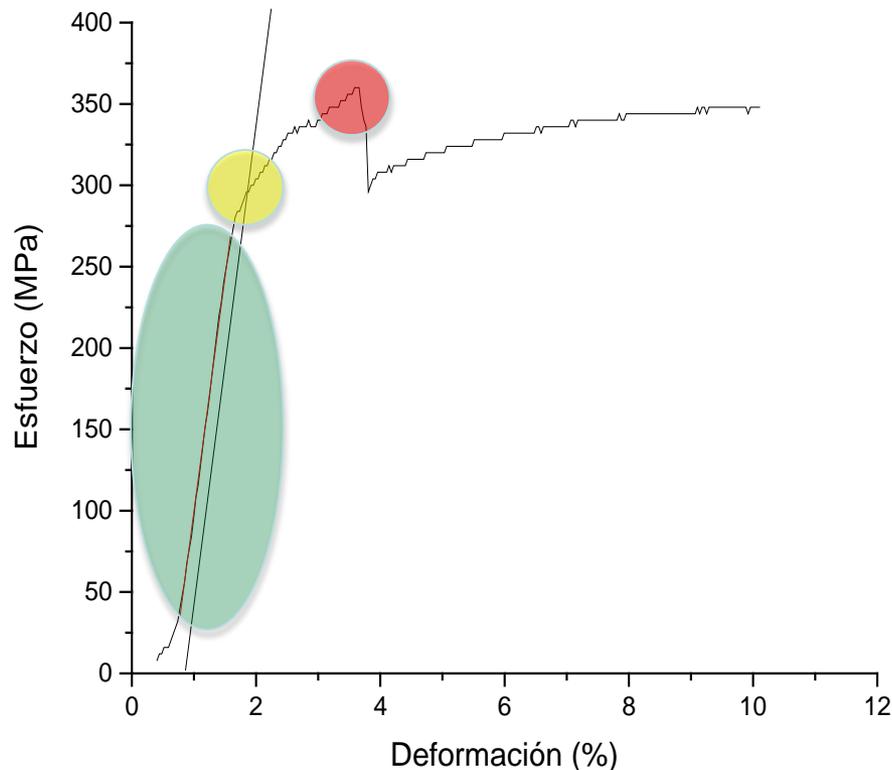
FABRICACIÓN

Configuración 2 y 3



ENSAYO DE TRACCIÓN

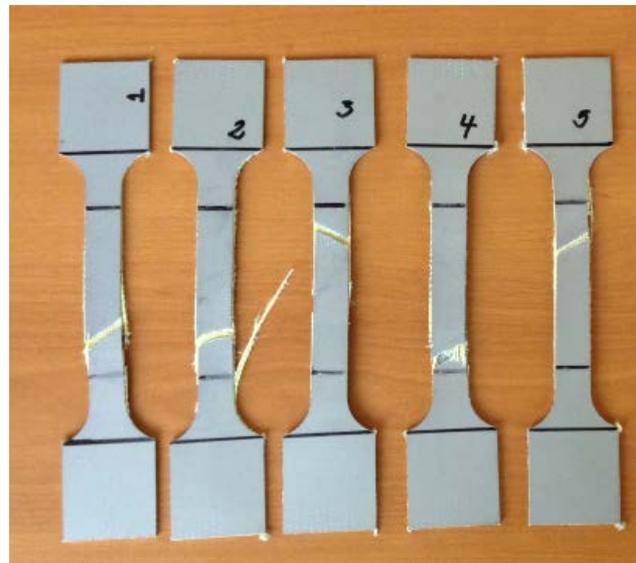
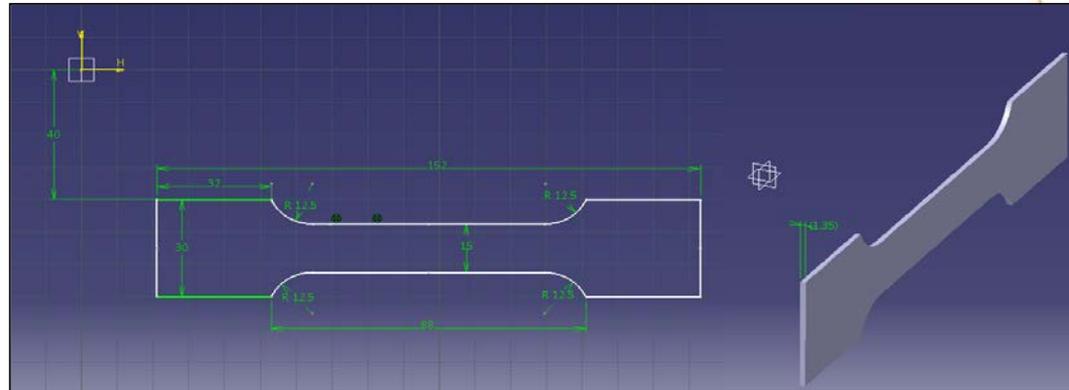
ASTM D3552-12, "Standard Test Method for Tensile Properties of Fiber Reinforced Metal Matrix Composites"



Ensayo de Tracción

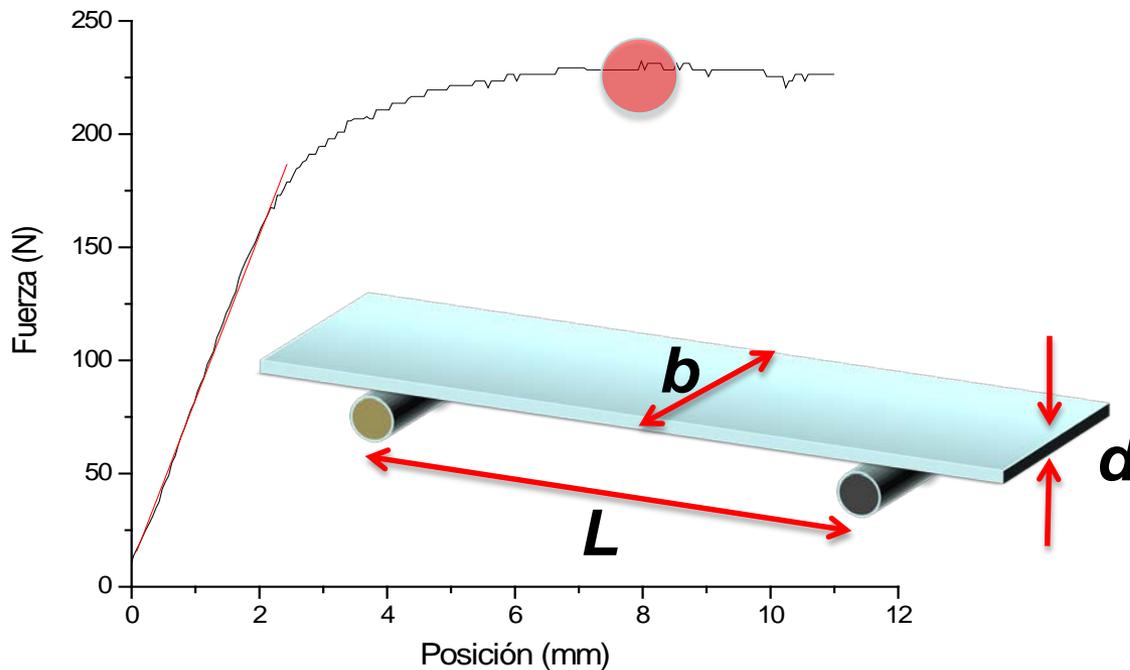
- Ensayo más común en materiales compuestos
- Representación en curvas Esfuerzo - Deformación
- Módulo de elasticidad
- Límite de Fluencia
- Esfuerzo tensil máximo

FABRICACIÓN DE PROBETAS PARA ENSAYO DE TRACCIÓN



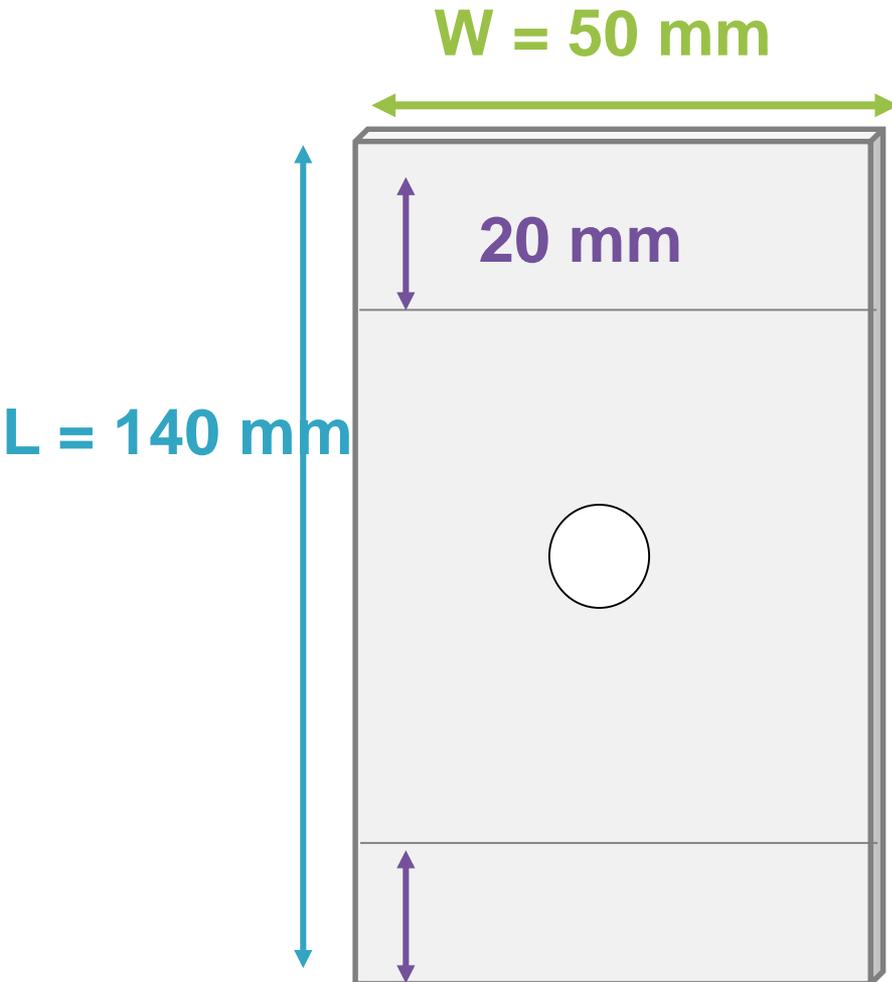
ENSAYO DE FLEXIÓN

ASTM D790-10 "Standard Test Methods for Flexural Properties of Unreinforced and Reinforced Plastics and Electrical Insulating Materials"



- Flexión de tres o cuatro puntos
- Representación por curva Fuerza-Deflexión
- Carga máxima
- Módulo de elasticidad

ENSAYO DE FATIGA

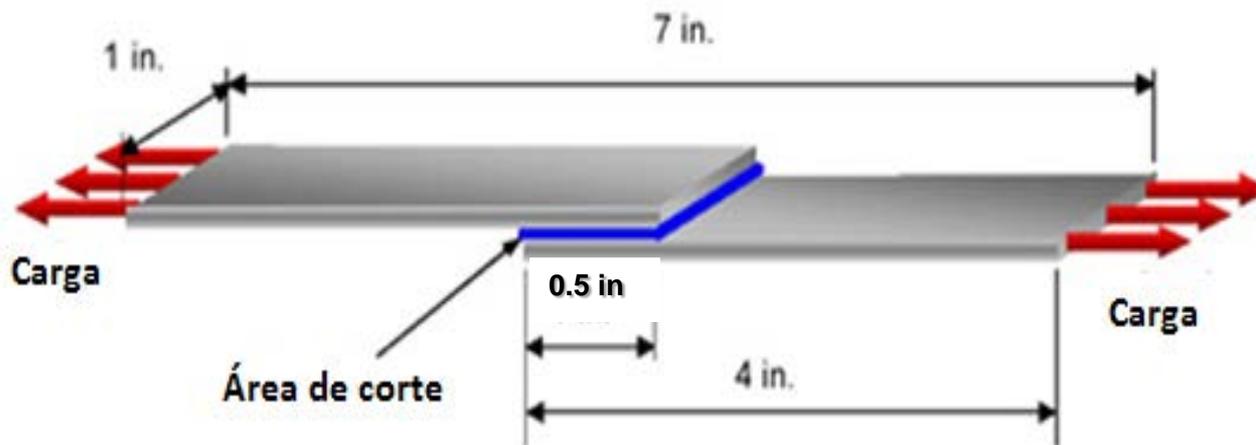


Norma ASTM E647
"Standard Test Method
for Measurement of
Fatigue Crack Growth
Rates",

ENSAYO LAP-SHEAR



- Esfuerzo de corte soportado por la resina
- Carga máxima
- Máximo esfuerzo de corte



RESULTADOS

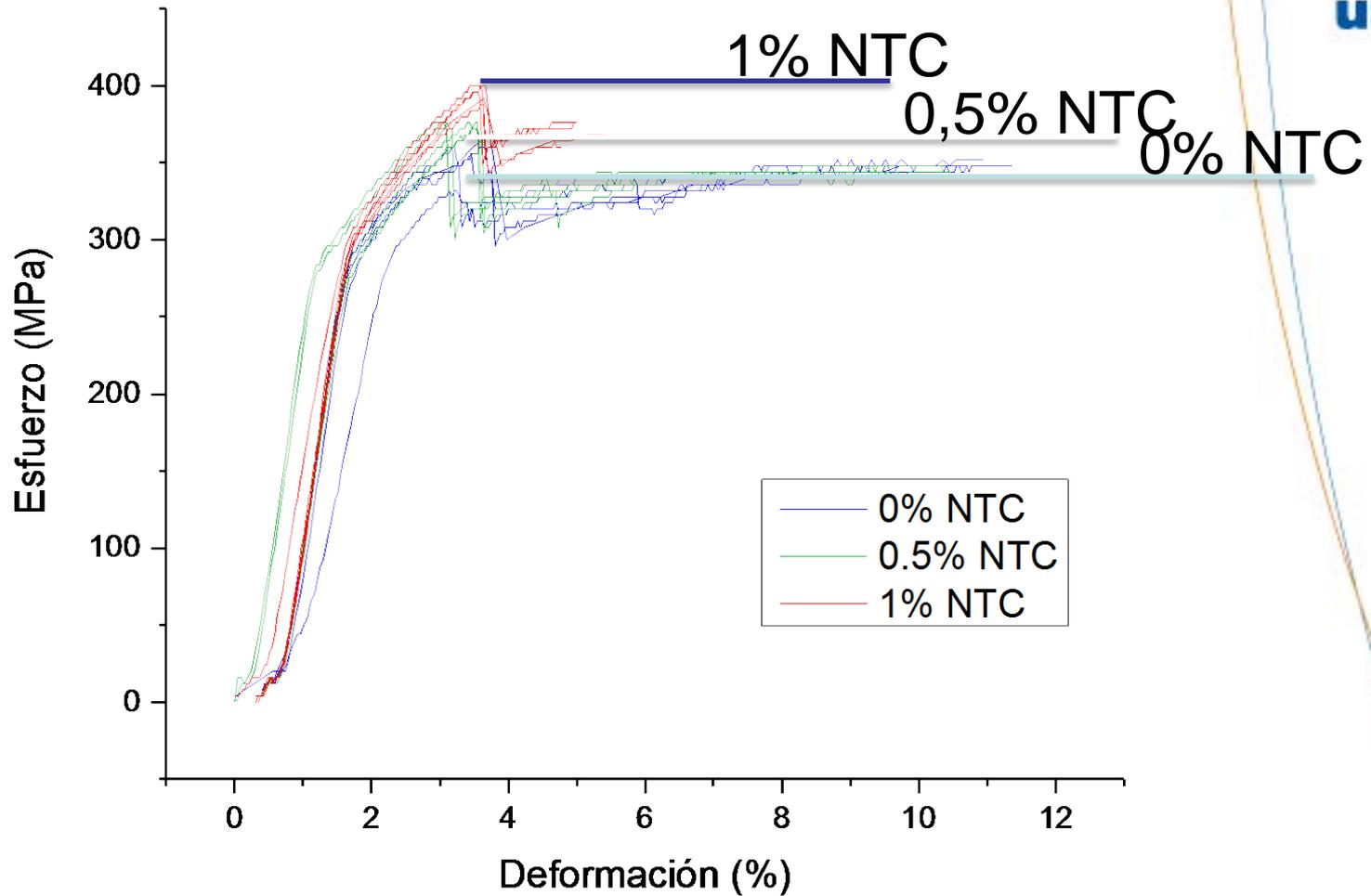
GLARE 0-0,5 y 1% NTC

Tracción, Flexión y Lap-Shear de GLARE

ARALL 0-0,5 y 1% NTC

Impacto balístico y Fatiga de ARALL

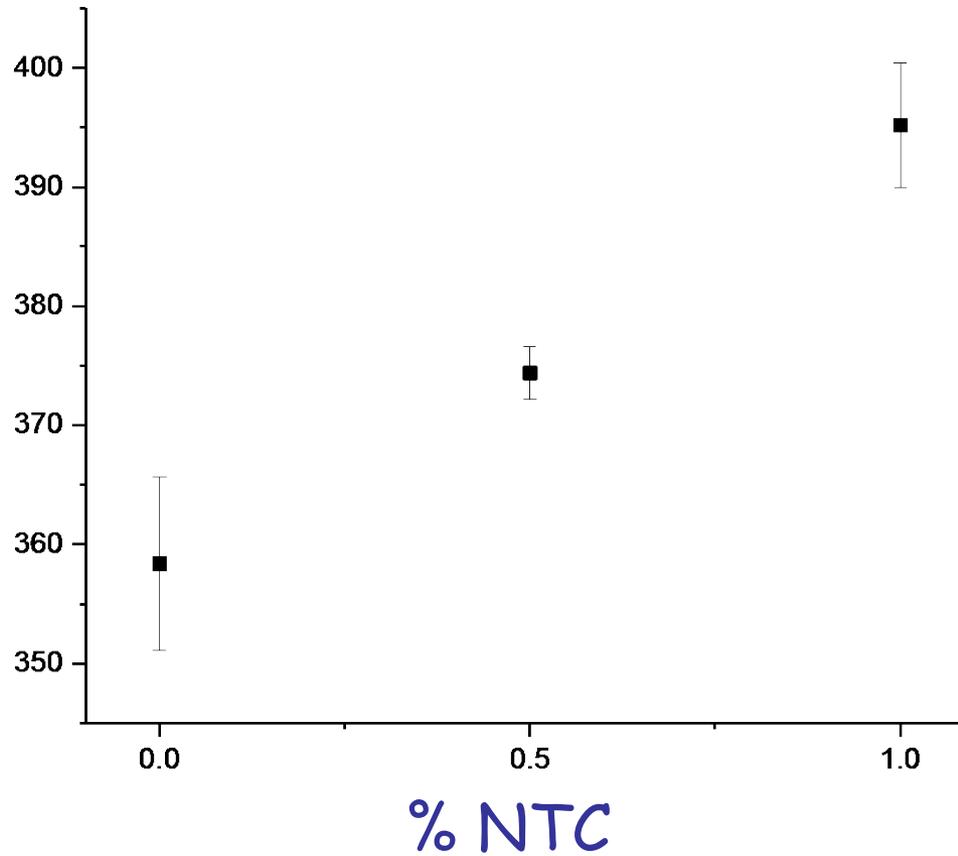
Resultados de ensayos de tracción en GLARE



Resultados de ensayos de tracción en GLARE



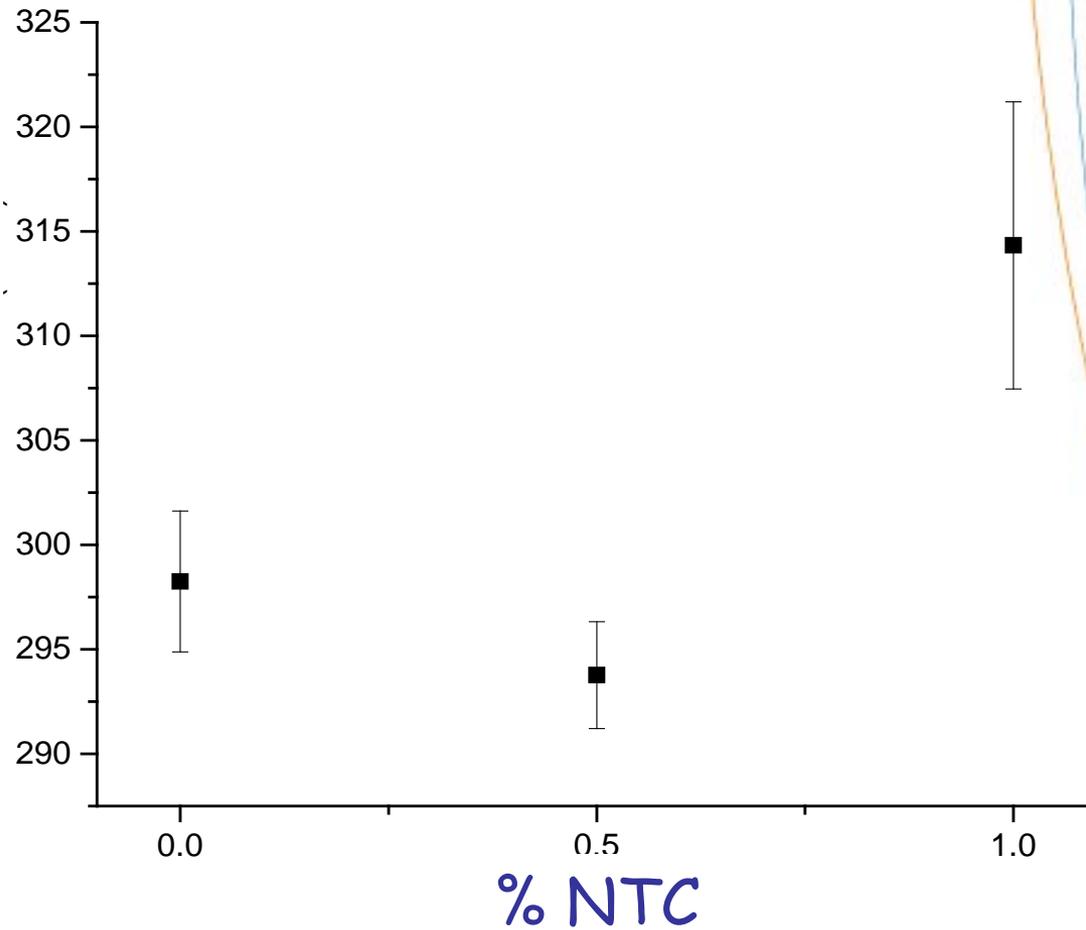
Máximo
esfuerzo
tensil (MPa)



Resultados de ensayos de tracción en GLARE



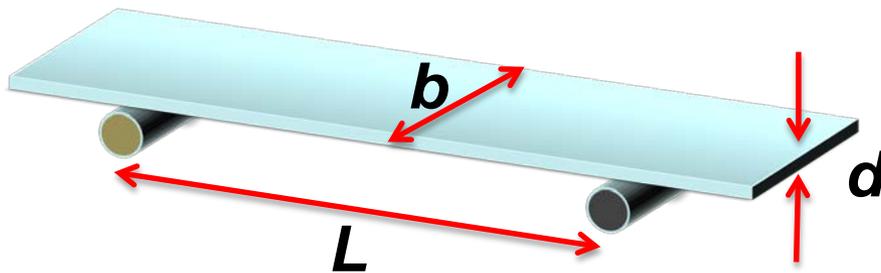
Límite de Fluencia



Resultados de ensayos de flexión en GLARE

Módulo de Elasticidad

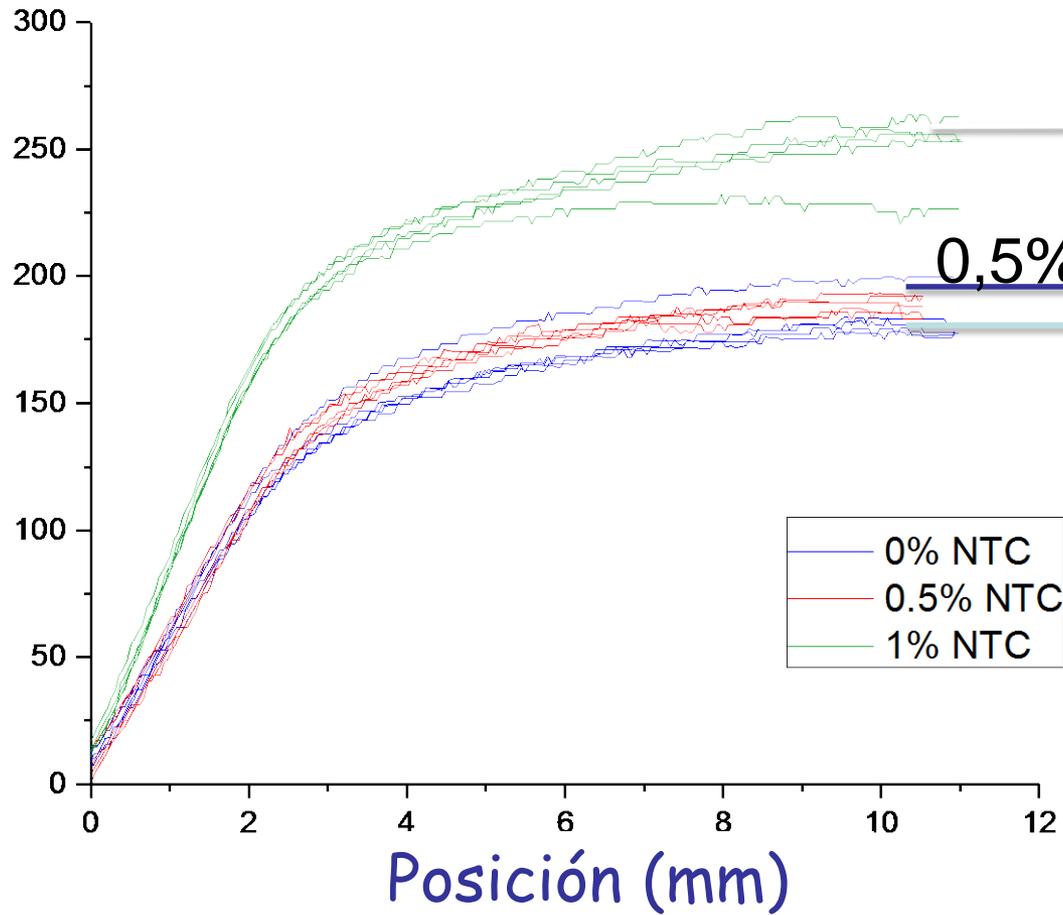
$$E_B = \frac{L^3 m}{4bd^3}$$



Resultados de ensayos de flexión en GLARE



Fuerza (N)

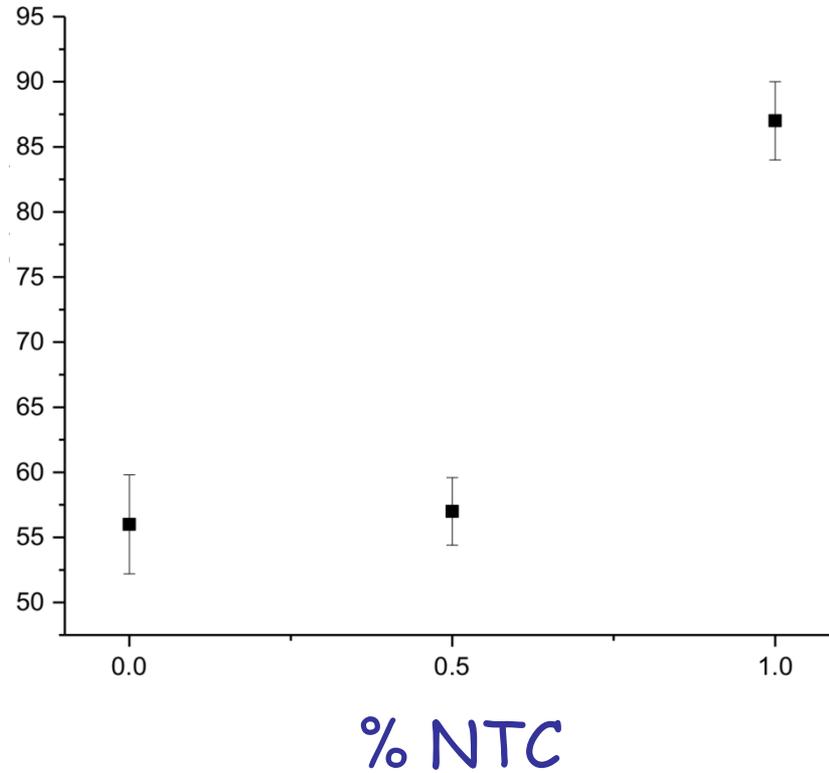


Resultados de ensayos de flexión en GLARE



Módulo de Young

Módulo de Young (GPa)

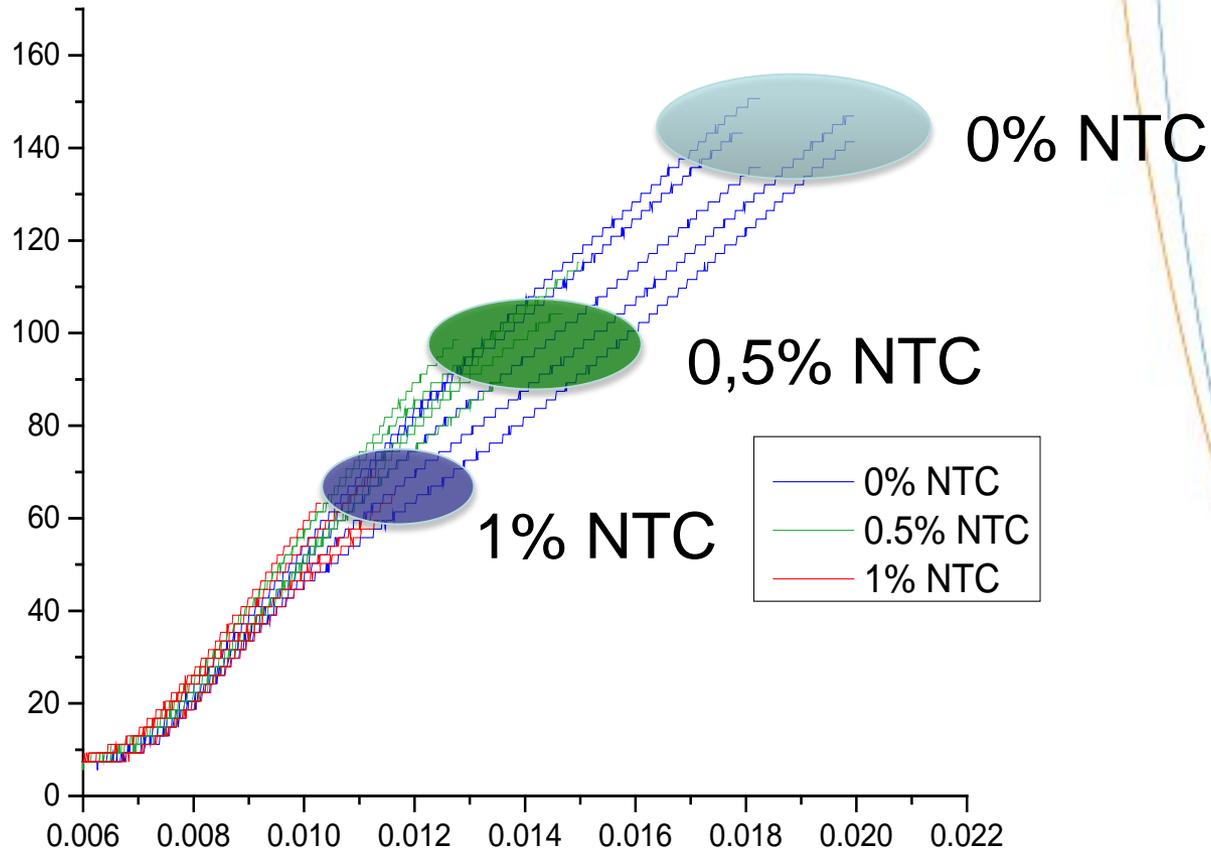


Resultados de ensayos de Lap-Shear en GLARE



Ensayo Lap-Shear

Esfuerzo (MPa)



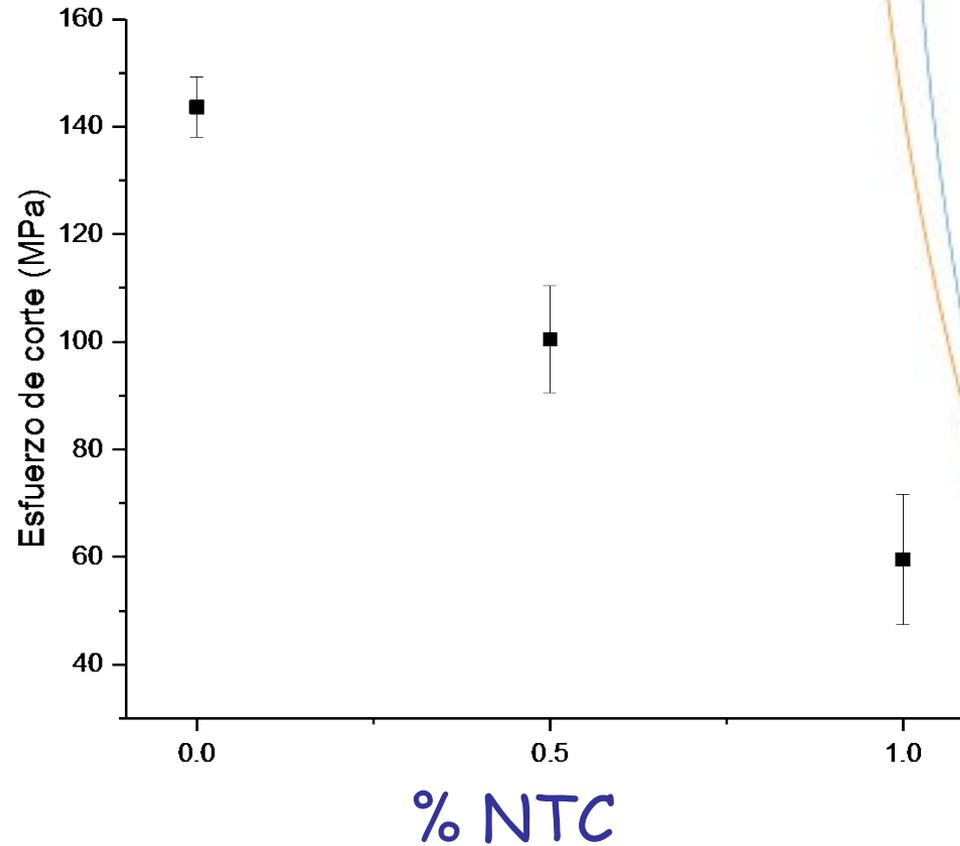
Deformación (%)

Resultados de ensayos de Lap-Shear en GLARE

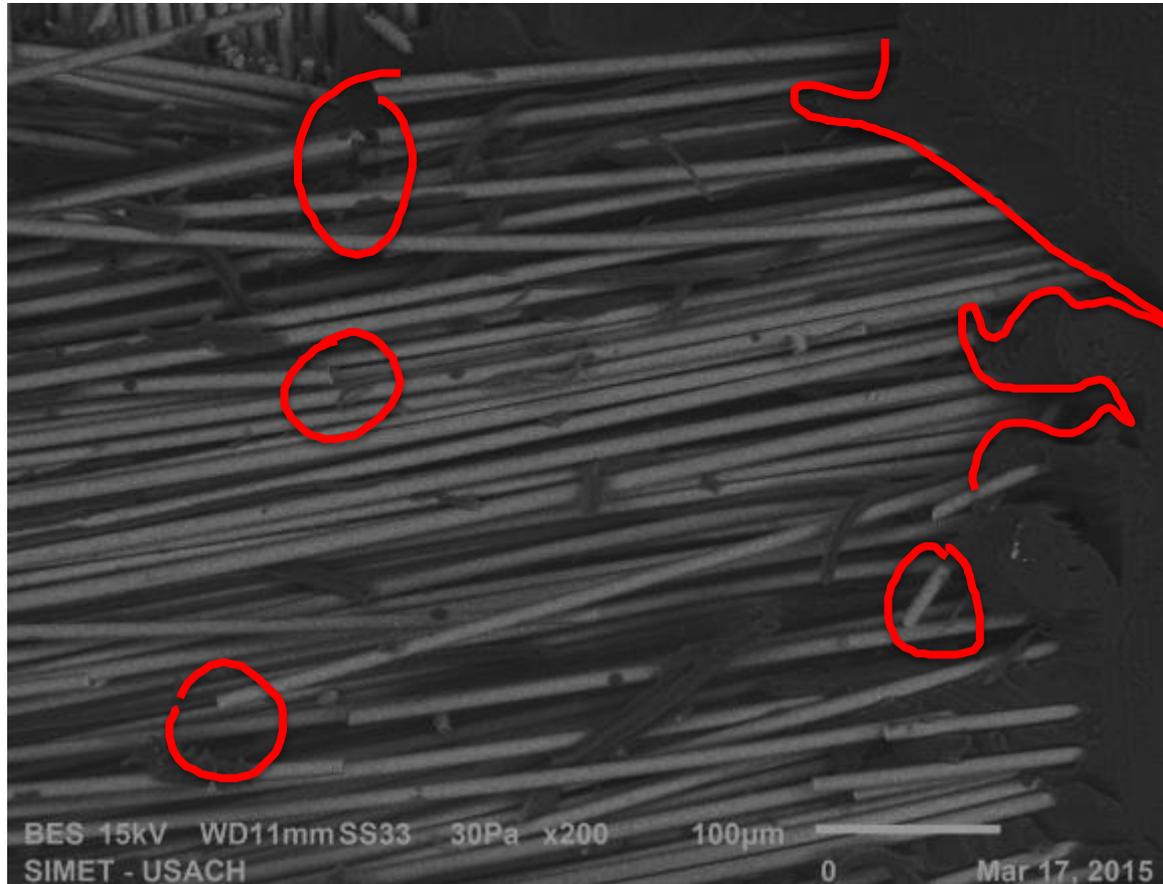


Ensayo Lap-Shear

Esfuerzo máximo (MPa)

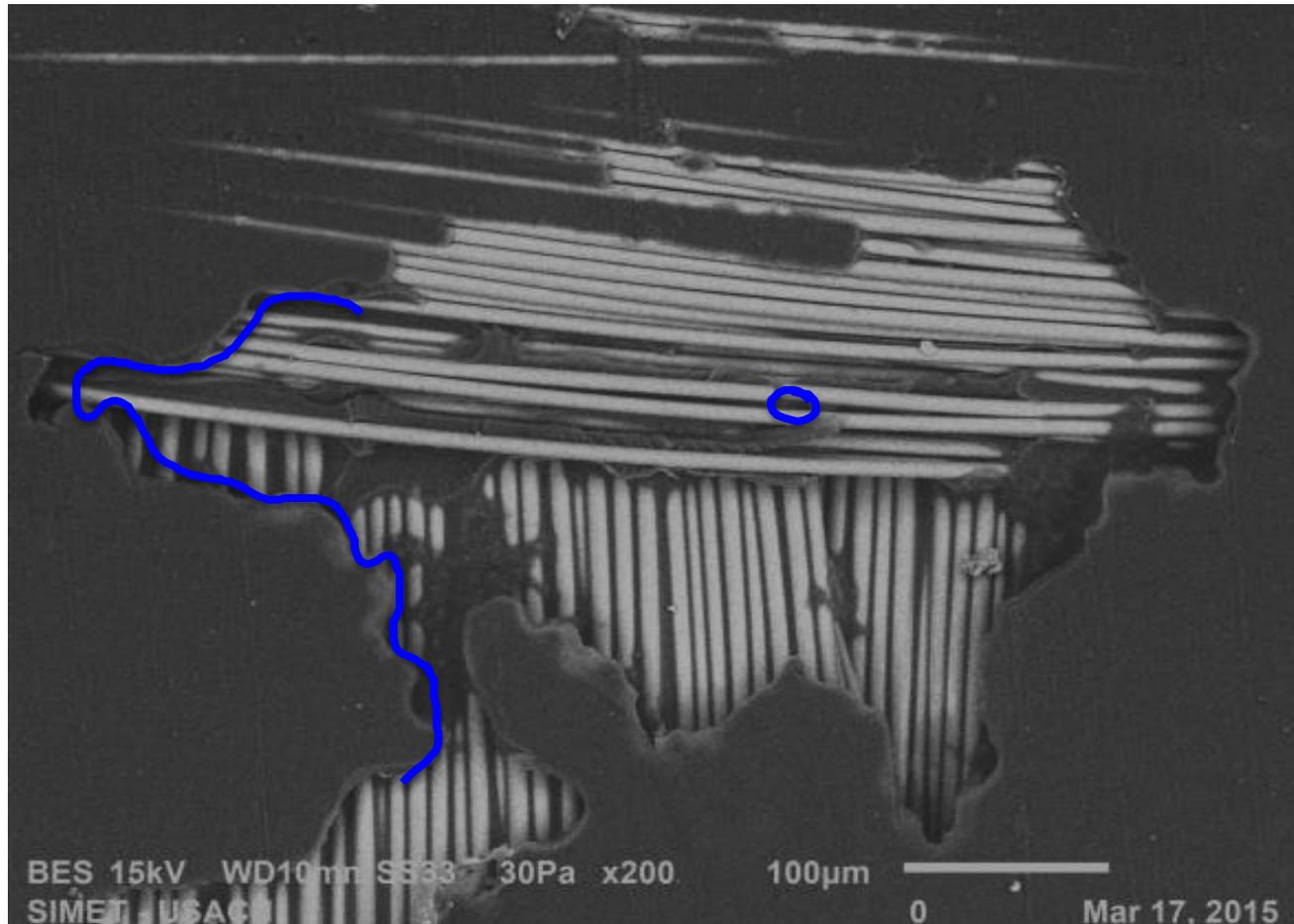


Análisis por microscopía electrónica de barrido en GLARE



Probeta de Lap-Shear 0% NTC a un aumento de 200X

Análisis por microscopía electrónica de barrido en GLARE

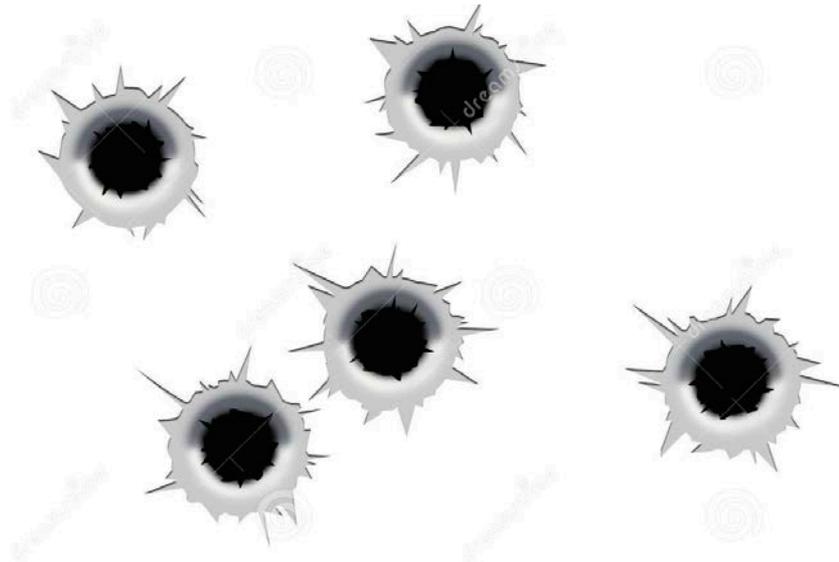


Probeta de Lap-Shear 1% NTC a un aumento de 200X

IMPACTO BALÍSTICO EN ARALL



Norma UL- 752 Nivel 8



IMPACTO BALÍSTICO Y FATIGA DE ARALL

Impacto Balístico

Norma UL- 752 Nivel 8

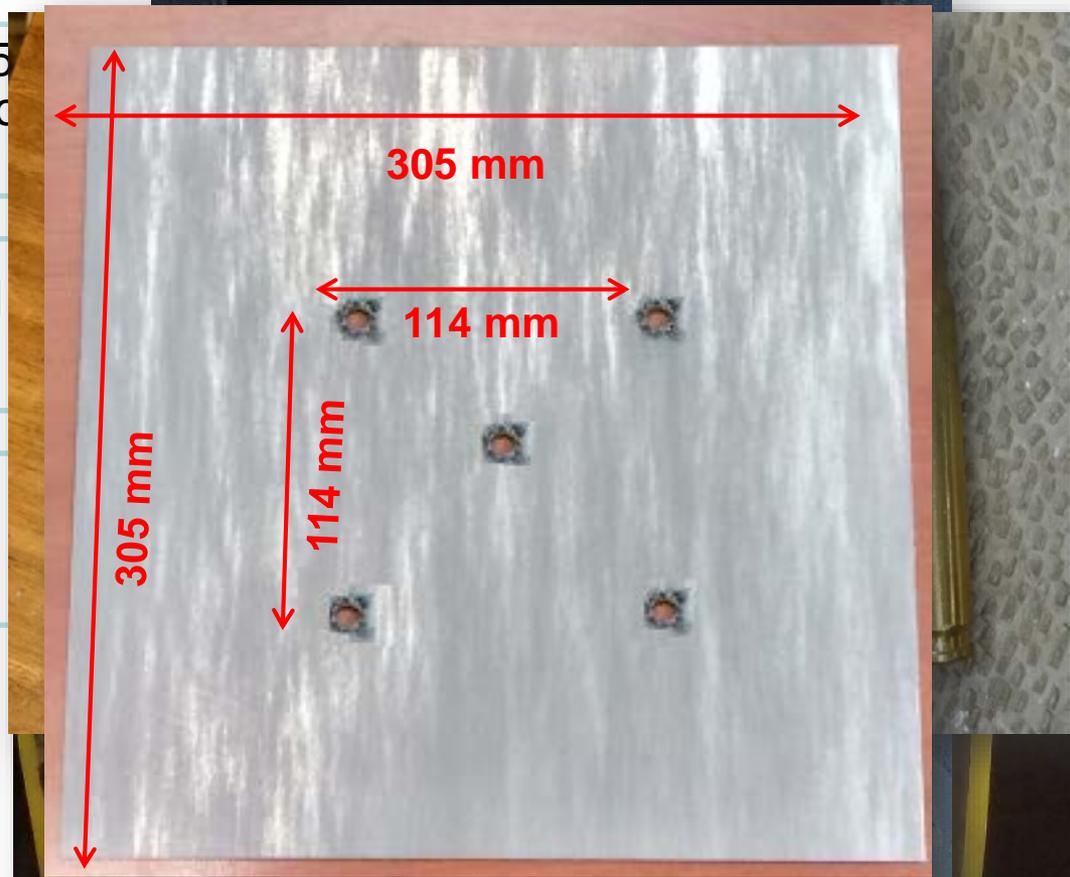
Munición 7,62x51 mm

Probeta de 305x305 mm

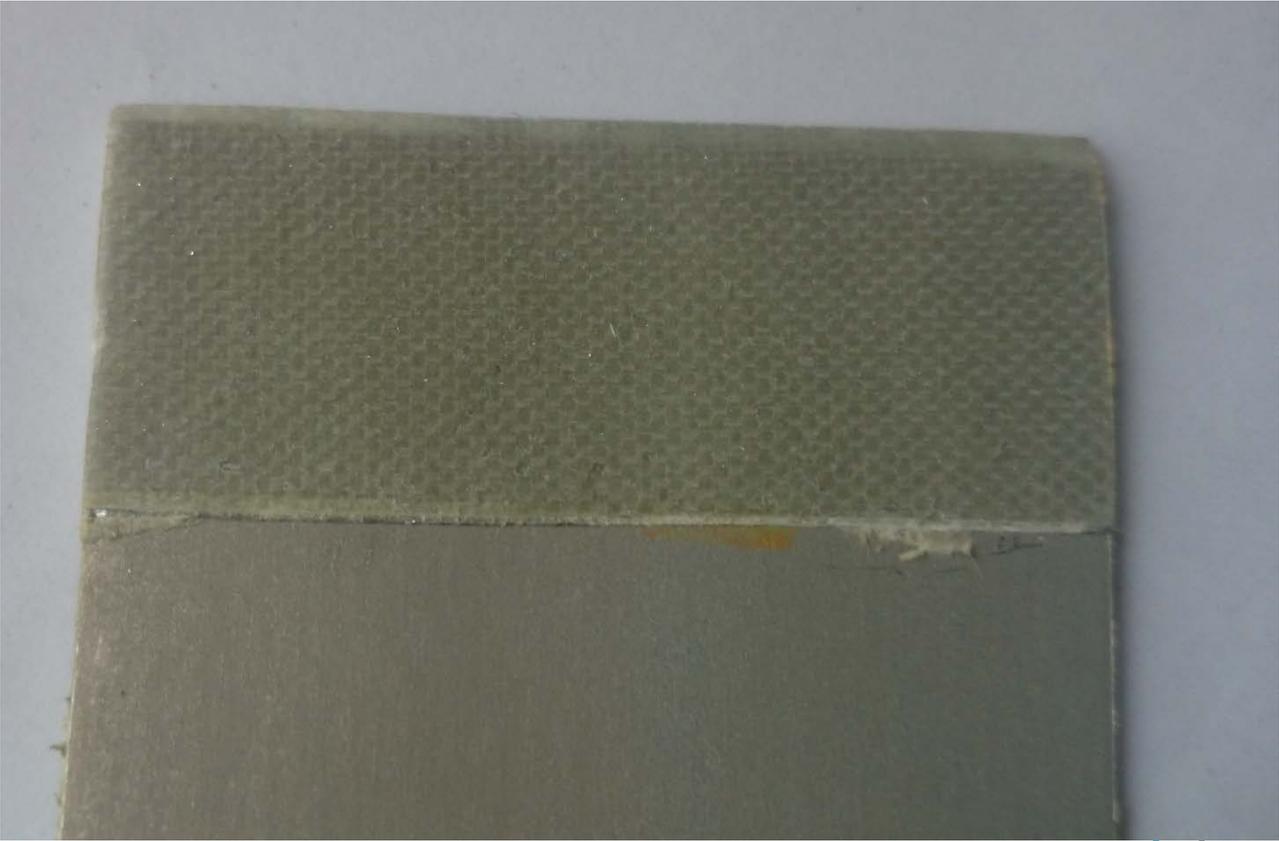
5 impactos

15 metro de distancia

Velocidad min 838 m/s



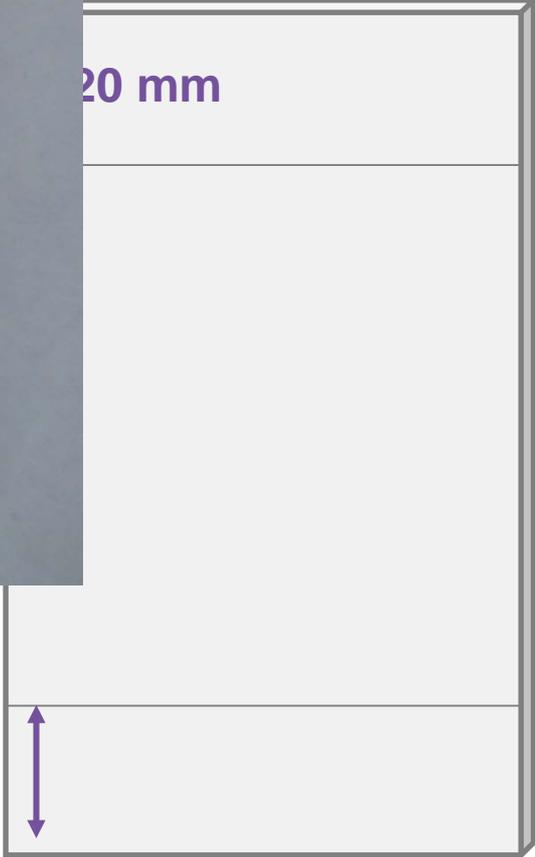
Diseño de probetas



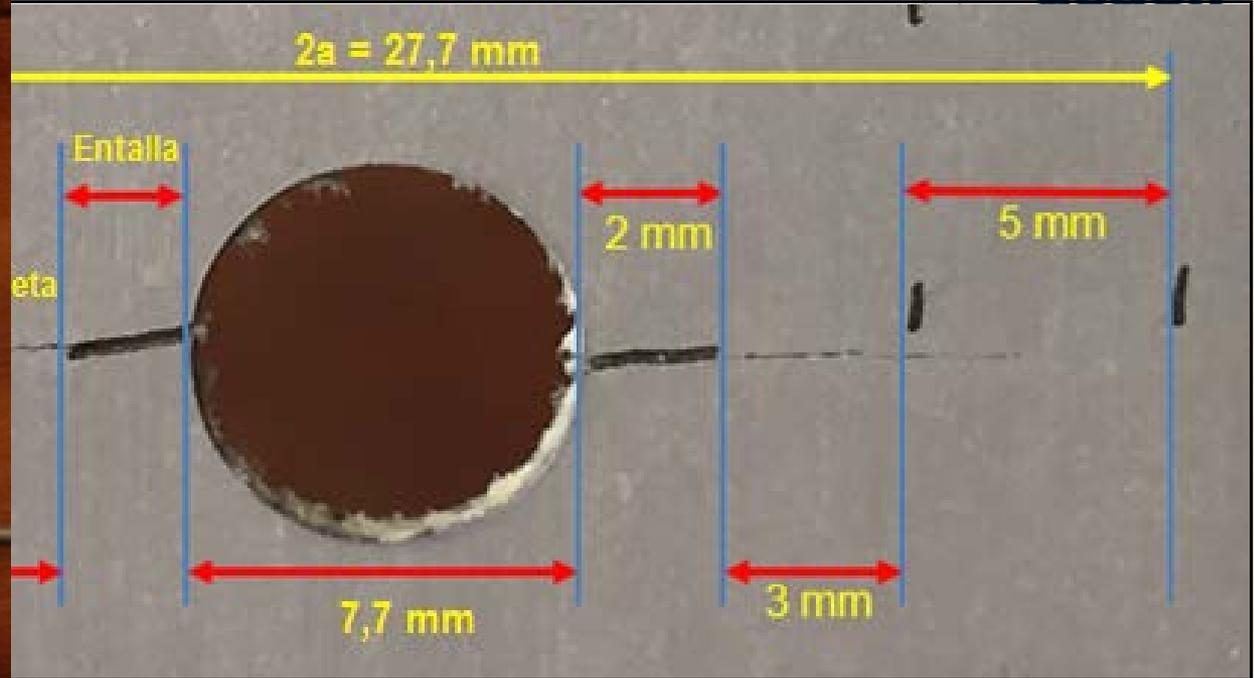
W = 50 mm



20 mm



Metodología de ensayo



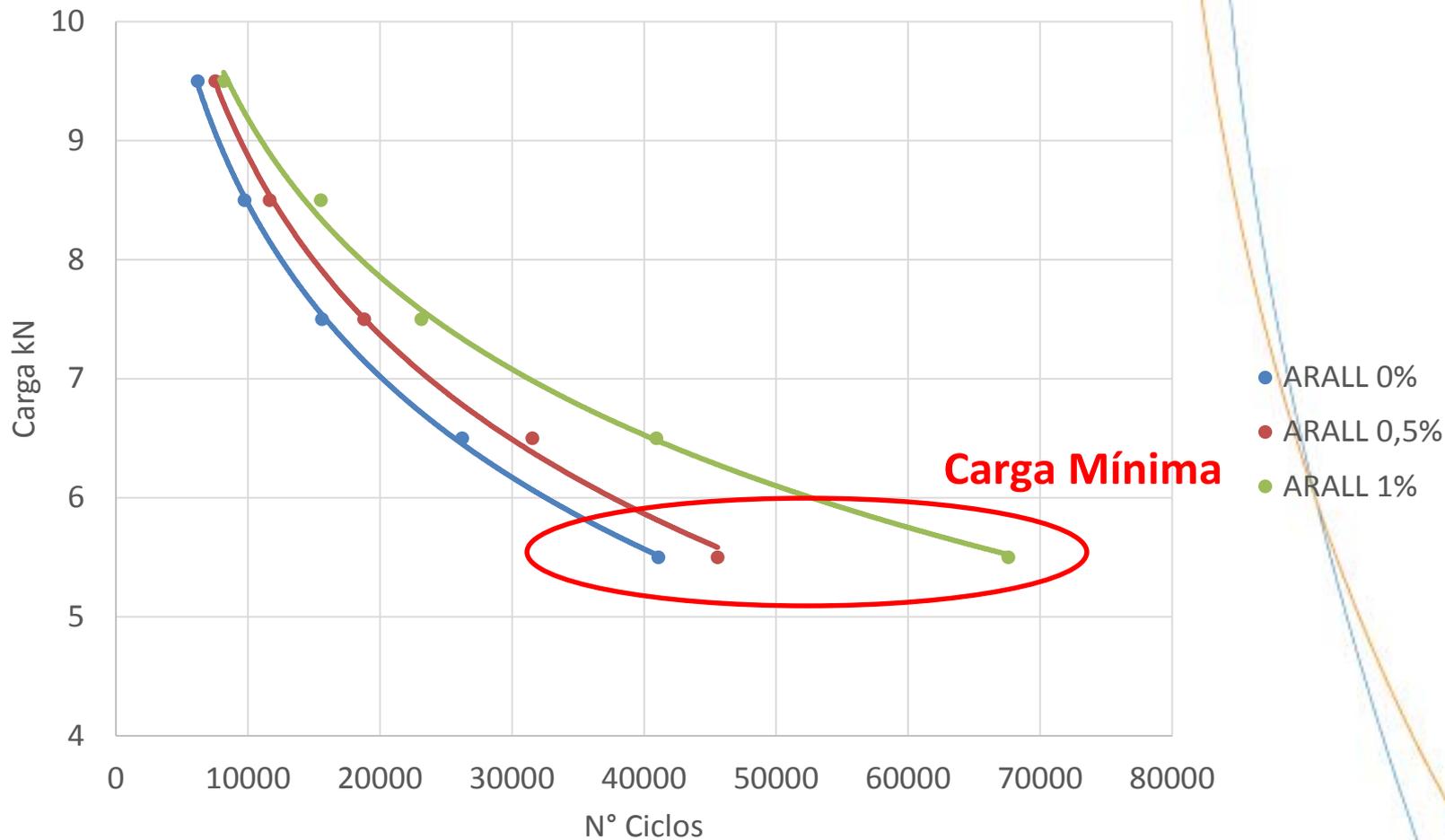
$$0,45W \leq 2a \leq 0,55W$$

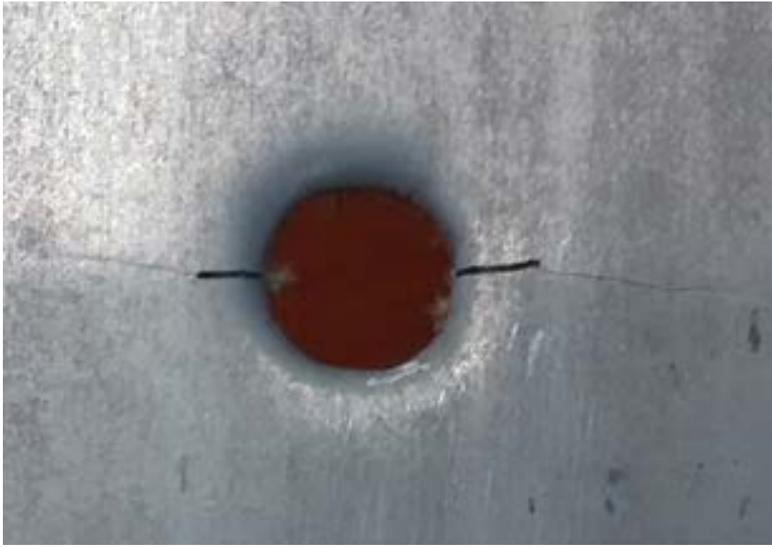
$$22,5\text{mm} \leq 2a \leq 27,5\text{mm}$$

Análisis y Resultados



ARALL sin impacto





0% NTC

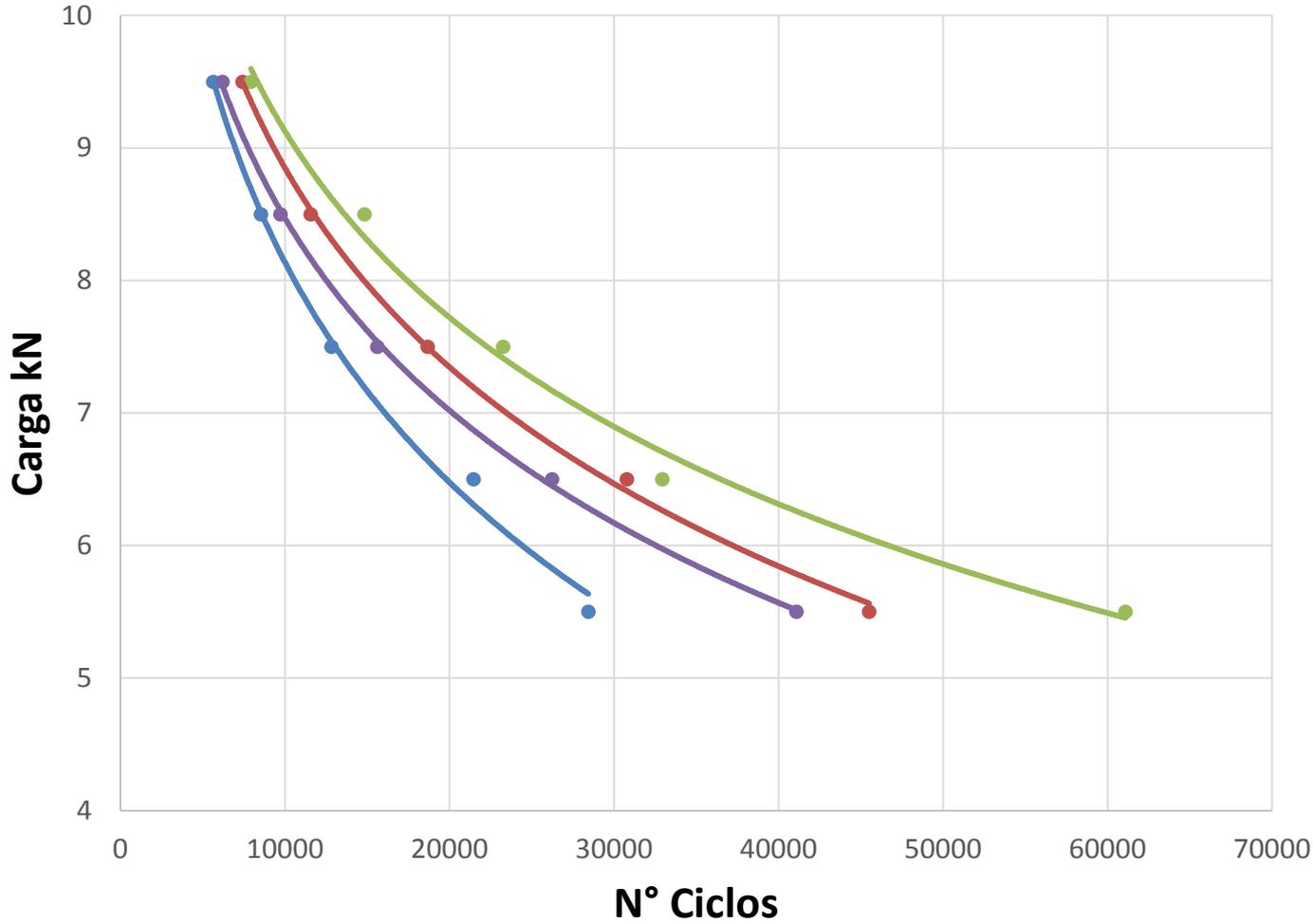


1% NTC

ARALL CON IMPACTO



ARALL con impacto



- ARALL 0%
- ARALL 0,5%
- ARALL 1%
- ARALL 0% Sin Impact

Conclusiones

Tanto en *GLARE* como en *ARALL*, la incorporación de NTC a la resina, mejora significativamente el desempeño de ambos materiales.

Se debe seguir investigando para averiguar aspectos importantes del sistema resina epóxica más nanotubos de carbono.



Trabajo futuro



Usar Grafeno como reforzante.

Alberto Monsalve, Luis Parra, Diego Baeza, Roberto Solís, Humberto Palza, Mechanical properties and morphological characteristics of ARALL reinforced with TRGO doped epoxy resin, Materia, Vol 57, N° 13, 223-232

Alberto Monsalve, Roberto Solís, Mauricio Díaz, Sebastián Carrasco, Alfredo Artigas, Multi-walled carbon nanotube reinforced polymer a bonded repair for Al 2024-T3 fatigue crack growth , Materia, Vol 57, N° 13, 233-239

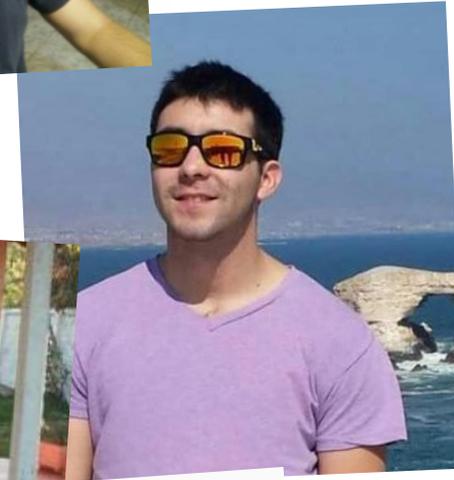
El equipo:

Felipe Morales
Andrea Maturana

Sebastián Carrasco
Mauricio Díaz

Allan Asenjo
Felipe Von Hausen
Christhoper Haertwig

Roberto Solís



AGRADECIMIENTOS

UNIVERSIDAD DE SANTIAGO DE
CHILE (USACH)

ACADEMIA POLITÉCNICA
AERONÁUTICA (APA)

AIR FORCE OFFICE FOR
SCIENCE RESEARCH (AFOSR)





Gracias por la atención